

Mapping recent lava flows at Westdahl Volcano, Alaska, using radar and optical satellite imagery

Zhong Lu^{a,*}, Russell Rykhus^{a,1}, Tim Masterlark^{a,2}, Ken G. Dean^{b,3}

^aU.S. Geological Survey, EROS Data Center, SAIC, 47914 252nd Street, Sioux Falls, SD 57198, USA

^bGeophysical Institute, University of Alaska-Fairbanks, P.O. Box 757320, Fairbanks, AK 99775-7320, USA

Received 24 September 2003; received in revised form 3 March 2004; accepted 14 March 2004

Abstract

Field mapping of young lava flows at Aleutian volcanoes is logistically difficult, and the utility of optical images from aircraft or satellites for this purpose is greatly reduced by persistent cloud cover. These factors have hampered earlier estimates of the areas and volumes of three young lava flows at Westdahl Volcano, including its most recent (1991–1992) flow. We combined information from synthetic aperture radar (SAR) images with multispectral Landsat-7 data to differentiate the 1991–1992 flow from the 1964 flow and a pre-1964 flow, and to calculate the flow areas (8.4, 9.2, and 7.3 km², respectively). By differencing a digital elevation model (DEM) from the 1970–1980s with a DEM from the Shuttle Radar Topography Mission (SRTM) in February 2000, we estimated the average thickness of the 1991–1992 flow to be 13 m, which reasonably agrees with field observations (5–10 m). Lava-flow maps produced in this way can be used to facilitate field mapping and flow-hazards assessment, and to study magma-supply dynamics and thus to anticipate future eruptive activity. Based on the recurrence interval of recent eruptions and the results of this study, the next eruption at Westdahl may occur before the end of this decade. © 2004 Elsevier Inc. All rights reserved.

Keywords: Lava flows; Satellite imagery; Mapping

1. Background

1.1. Mapping lava flows

Accurately mapping the aerial extent and thickness of lava flows is required to calculate the volume of an eruption. Flow volumes are used to constrain models of the magma supply and plumbing system, which cannot be directly observed (e.g., Crisp, 1984; Dvorak & Dzurisin, 1993; Rowland et al., 1999; Wadge, 1977). Lava flows can be mapped directly in the field or with remote sensing techniques (e.g., Abrams et al., 1996; Dean et al., 2002; Legeley-Padovani et al., 1997; Lu et al., 2000a, 2003a; Rowland et

al., 1994; Zebker et al., 1996). The remote locations of most Alaskan volcanoes result in expensive and complex logistics that hinder lava flow mapping in the field. Therefore, remote sensing plays a critical role in determining the extent of lava fields at Aleutian volcanoes.

Optical satellite images have been successfully used to map lava flows and their associated spectral and morphological properties (e.g., Abrams et al., 1996; Legeley-Padovani et al., 1997). Satellite data in the visible, infrared, and thermal wavelength regions contain reflectance and emittance information about lava surfaces of different origin and age, and therefore can be used to distinguish different lava flows. However, in optical images, it can be difficult to distinguish cooled, fresh flows from other young flows that have not been modified by weathering due to the similarity in their chemical composition and morphology. In addition, mapping based on optical satellite imagery requires that the area of interest be cloud-free and the data be acquired during or shortly after the eruption. In the Aleutian volcanic arc (Fig. 1), nearly persistent cloud cover precludes acquisition of useful optical satellite images for a particular time period. In the past 30 years, only a few cloud-free images

* Corresponding author. Tel.: +1-605-594-6063; fax: +1-605-594-6529.

E-mail addresses: lu@usgs.gov (Z. Lu), rykhus@usgs.gov (R. Rykhus), masterlark@usgs.gov (T. Masterlark), ken.dean@gi.alaska.edu (K.G. Dean).

¹ Tel.: +1-605-594-6121; fax: +1-605-594-6529.

² Tel.: +1-605-594-2847; fax: +1-605-594-6529.

³ Tel.: +1-907-474-7364; fax: +1-907-474-7314.

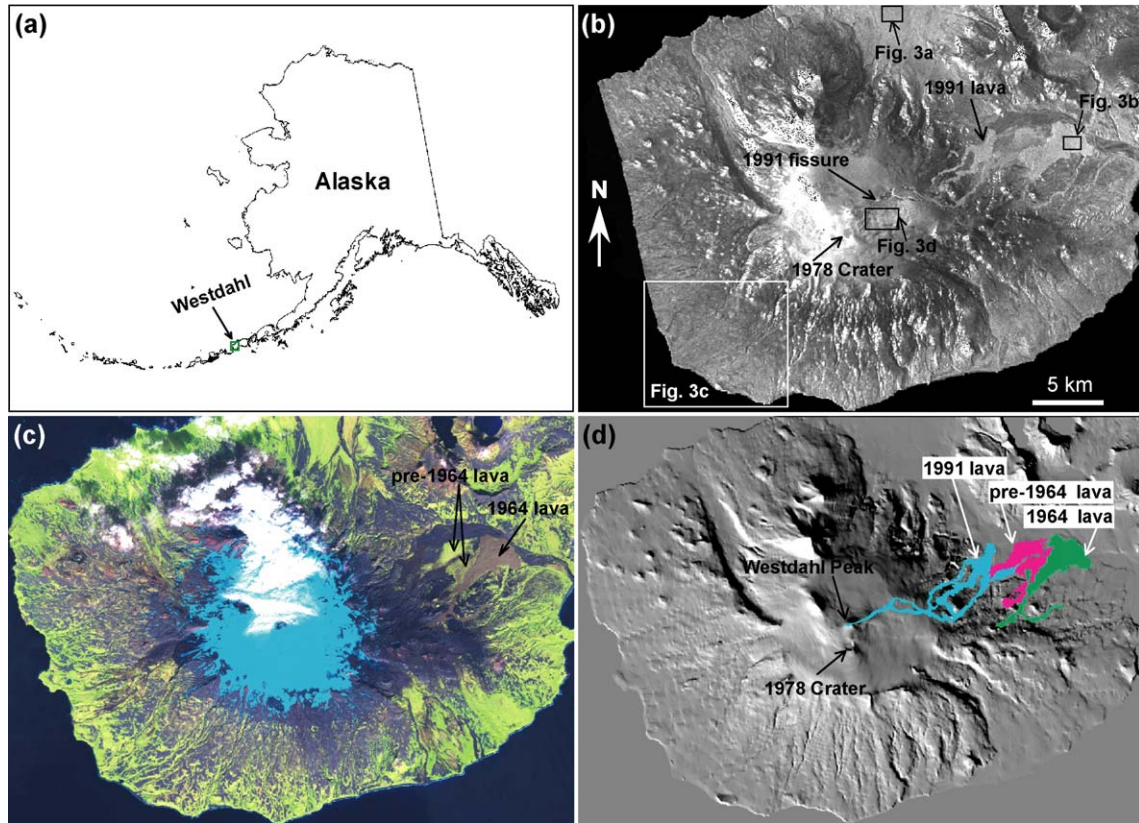


Fig. 1. (a) Map of Alaska showing the 2500-km-long Aleutian volcanic arc. The small rectangle indicates the locations of (b)–(d). (b) SAR image of Westdahl Volcano acquired by ERS-1 on February 9, 1992, shortly after the end of the 1991–1992 eruption. The small boxes outline areas corresponding to the histograms in Fig. 3a–d. (c) Color composite of Landsat-7 imagery created from bands 5, 4, and 3 as red-green-blue channels, respectively. The Landsat-7 ETM+ imagery was acquired on September 27, 2000. (d) A shaded-relief image of Westdahl Volcano based on a USGS NED DEM. The extents of the 1991–1992 lava flow, the 1964 lava flow, and the pre-1964 lava flow were mapped with both SAR and optical images.

have been acquired for most of the Aleutian volcanoes (<http://Glovis.usgs.gov>).

Synthetic aperture radar (SAR) images have also been used to map lava flows (e.g., Dean et al., 2002; Gaddis et al., 1990; Lu et al., 2000a, 2003a; Rowland et al., 1994, 1999; Zebker et al., 1996). SAR backscattering represents the amount of energy reflected back to the sensor from each resolution element of the imaged surface. Backscatter is the coherent sum of reflected energy from individual scatterers in each resolution element, which are typically sized on the scale of the SAR wavelength (from several centimeters to tens of centimeters). In addition to image geometry and sensor characteristics, SAR backscattering generally is controlled by terrain slope, surface roughness, and dielectric constant (primarily controlled by moisture) (Ulaby et al., 1986). Three techniques have been used to map the extent of lava flows with SAR imagery. The first constitutes the use of interferometric or stereoscopic SAR images (e.g., Hensley et al., 2001; Toutin, 1996) to produce digital elevation models (DEMs) that represent the topography of the volcano before and after the eruption. Lava flows can thus be mapped by subtracting pre- and post-eruption DEMs (e.g., Lu et al., 2003a; Rowland et al., 1999). This approach requires DEMs with vertical accuracy of at least several

meters. It has the advantage of measuring both the area and thickness of a flow and thus its volume. However, SAR images suitable for producing DEMs are not always available for a variety of reasons, primarily the lack of SAR data with appropriate orbital geometry (e.g., Lu et al., 2003a). The second technique is based on changes in SAR backscattering (both amplitude and phase data) or interferometric coherence between two scenes (Lu et al., 2000a; Zebker et al., 1996). This approach requires that changes in the SAR backscattering signal be relatively small in areas surrounding the fresh lava flows. For this reason, the imaging geometry and flight passes of the SAR imagery must be nearly identical. Furthermore, temporal separation of the SAR images should be as short as possible (approximately days) to minimize the reduction of radar coherence caused by environmental changes in areas not covered by fresh lava. The third technique utilizes the amplitude data of single or multiple SAR images to map the fresh lava flows. This approach requires that the amplitude of the SAR backscattering signal from fresh lava be distinct from that of the surrounding terrain (e.g., Dean et al., 2002; Gaddis et al., 1990; Rowland et al., 1994, 1999). Multiple images can reduce the noise in data and improve the accuracy of a lava flow map.

1.2. Westdahl Volcano

Westdahl is a young glacier-capped shield volcano located at the west end of Unimak Island in the central part of the Aleutian volcanic arc, about 85 km southwest of the tip of the Alaska Peninsula (Fig. 1). The Westdahl edifice is composed of a thick sequence of pre-glacial basalt lava flows. Westdahl Peak, an active center, is on a gently sloping plateau that might represent the surface of a truncated ancestral cone of Pleistocene age or older (Miller et al., 1998). Eruptions at or near Westdahl Peak were documented in 1795, 1796, 1820, and 1827–1830 (Miller et al., 1998). However, many other eruptions could have gone undetected due to the volcano's remote location. Westdahl was frequently active during the latter half of the 20th century with documented eruptions in 1964, 1978, and 1991–1992.

In March–April 1964, a fissure eruption at Westdahl produced a lava flow that descended the northeast flank of the volcano (Wood & Kienle, 1990). A volcanian eruption in 1978 through glacial ice produced a crater, about 1.5 km in diameter and 0.5 km deep, near the source vent of the 1964 eruption and is now mostly filled with snow and ice (Global Volcanism Network, 1978). During the 1978 eruption, ash was reported to have reached altitudes of 10 km, and ash deposits with an estimated thickness of 18 cm were observed about 15 km southwest of the summit (Global Volcanism Network, 1978). The eruption also produced a lahar that traveled down the southwest flank of the volcano to the sea. The thickness of the lahar deposit ranged from about 50 cm on the upper slopes of the volcano to 1–3 m near the coast (Global Volcanism Network, 1978).

The most recent eruption of Westdahl was first reported by pilots, who observed a fissure erupting through ice on November 29, 1991. The fissure extended 8 km eastward from a point near Westdahl Peak (Fig. 1), and ash venting occurred discontinuously along most of the fissure length. Lava fountaining was observed along the lower portion of the fissure and fed lava flows that descended the volcano's eastern flank. During the course of the eruption, dramatic lava fountaining and phreatic activity produced ash plumes that rose to an altitude of 7 km, prompting the US Federal Aviation Agency to divert air traffic (Dean et al., 2002). Activity declined in mid-December and ceased by mid-January 1992 (Miller et al., 1998).

2. Mapping lava flows using both SAR and optical images

Based on an oblique aerial photograph, the 1991–1992 lava flow was estimated to be about 7 km long, up to 3 km wide, and 5–10 m thick, with an area of about 5 km² (T. Neal, personal communication, 2002). These estimates have since been refined using SAR imagery. Over gently sloping terrain, the SAR backscattering signal is primarily con-

trolled by surface roughness. Surfaces that are rough at scales comparable to or larger than the radar wavelength have large radar cross-sections and appear bright in SAR images. The rough *aa* texture of the 1991–1992 flow makes it a radar-bright feature. Rowland et al. (1994) calculated the area of 1991–1992 flow to be 6.3 km² by using a ERS-1 SAR amplitude image acquired on February 27, 1992, an oblique aerial photograph acquired in March 1992, and an X-band radar image acquired in 1982. The authors did not present a map showing the inferred extent of the 1991–1992 or other young lava flows. Dean et al. (2002) used multiple SAR amplitude images to map the 1991–1992, 1964, and a pre-1964 lava flow. They calculated the area of the 1991–1992 flow to be 3.79 km². This estimate is significantly smaller than that obtained by Rowland et al. (1994) (3.79 versus 6.3 km²). The 1991–1992 flow, 1964 flow, and a pre-1964 flow have similar radar cross-sections, so differentiating them on the basis of SAR imagery alone is difficult. We suspect that this difficulty contributed to the discrepancy between earlier estimates of the 1991–1992 flow extent. In this paper, we use both radar and optical satellite imagery to map the 1991–1992, 1964, and pre-1964 lava flows, and to estimate the volume of 1991–1992 flows based on difference in DEMs.

Westdahl's upper flanks are typically covered with snow and ice from October through June, and the summit of the volcano remains covered throughout the year. Therefore, mapping lava flows on Westdahl's upper flanks requires acquisitions of satellite data (either radar or optical imagery) during or shortly after an eruption. Persistent cloud cover makes obtaining a useful optical satellite image at such times unlikely, but SAR sensors can provide timely imagery regardless of weather conditions. It is therefore possible to separate fresh lava from the surrounding snow and ice in the summit and upper flanks of the volcano using SAR imagery. However, young lava flows (e.g., extruded in 1991–1992) on the lower flanks and at the base of the volcano can have a surface roughness similar to adjacent older flows (e.g., extruded in 1964). For this reason, it is generally difficult to differentiate flows on the lower parts of the volcano if only single-frequency, single-polarization SAR data are used. In contrast, the multispectral capabilities of optical satellite imagery allow for the discrimination of lava flows based on differences in the flow composition and/or vegetation characteristics. If optical images are acquired a few years after an eruption, the youngest lava flow should be distinguishable from other relatively young flows based on differences in vegetation cover. By utilizing both SAR and optical imagery, we were able to differentiate and map the extent of young lava flow fields on both the upper and lower parts of Westdahl Volcano. We used this approach to map the 1991–1992, 1964, and pre-1964 flows. In addition, we differenced two DEMs, representing the topography of the volcano before and after the 1991–1992 eruption, to estimate the thickness of the 1991–1992 lava flow.

3. Data analysis

Three types of data were used to map recent lava flows at Westdahl: SAR amplitude images, a Landsat-7 multispectral image, and digital elevation models (DEMs). The first data set consists of six ERS-1 SAR images (Table 1) acquired from January 19 through February 9, 1992, shortly after the end of the 1991–1992 eruption. These images were acquired by the European ERS-1 satellite during the 3-day repeat pass phase. Multiple SAR data are used to reduce the speckle noise in the SAR images. The images were geo-referenced to the Universal Transverse Mercator (UTM) system based on a DEM and the SAR imaging geometry. Fig. 1(b) shows the amplitude image acquired on February 9, 1992 (Table 1). Because the fissures and lava channels from the 1991–1992 eruption are much rougher than the surrounding snow and ice, they are readily distinguished in the SAR image. On the upper flank of the volcano, the 1991–1992 flow can be traced downslope due to its relatively bright backscattering relative to that of adjacent flows. However, on the lower flank and near the base of the volcano, the backscattering from the 1991–1992 flow is not easily distinguishable from that of its surroundings (Fig. 1b).

The second data set includes a multispectral satellite image acquired on September 27, 2000 by Landsat-7 (NASA, 1999) (Fig. 1c). This Landsat-7 image has the least cloud cover among all of the Landsat data acquired over Westdahl Volcano in the arctic summers of the last 30 years (<http://www.Glovis.usgs.gov>). Landsat-7 acquires images at visible, near-infrared, and thermal wavelengths, which are very useful for characterizing vegetation and land cover. The Landsat-7 image (Fig. 1c) was co-registered with the SAR images and a color-composite image was created by assigning bands 5, 4, and 3 to red, green, and blue, respectively (Fig. 1c). Band 5 records the near-infrared part of the spectrum (1.55–1.75 μm), which is sensitive to the moisture content of soil and vegetation (Sabins, 1997). Band 4, another near-infrared channel (0.76–0.90 μm), is useful for mapping biomass content. Band 3 is a visible channel (0.63–0.69 μm) that is sensitive to chlorophyll absorption and helps discriminate among vegetation types. In Fig. 1(c), bright blue areas represent ice and snow and white bands represent clouds over the central and northwestern parts of the volcano. Non-vegetated areas, such as the 1991–1992 lava flow,

appear black or purple, whereas vegetated areas appear as shades of green. The fissures and irregular channels from the 1991–1992 eruption are buried by snow and ice in the Landsat-7 image, and therefore the 1991–1992 lava flow cannot be differentiated from its surroundings on the upper flank of the volcano. In contrast, the distal end of the 1991–1992 flow is easily distinguishable from the lava flows of previous eruptions on the volcano's lower flank (Fig. 1c).

The final data set includes DEMs from the US Geological Survey (USGS) National Elevation Database (NED) and the Shuttle Radar Topography Mission (SRTM). Both data sets are available online at <http://edc.usgs.gov/products/elevation.html>. The NED DEM is based on contour data supplemented with photogrammetric data acquired in 1970–1980s, has a horizontal resolution of about 60 m, and a root-mean-square (RMS) vertical error of 15 m (Gesch, 1994). The NED DEM has a horizontal datum of the North American Datum 1927 (NAD 27) and vertical datum of North American Vertical Datum 1988 (NAVD 88). The 1-arc-second (about 30 m) SRTM DEM, acquired in February 2000, has a relative vertical accuracy better than 10 m and an absolute vertical accuracy better than 16 m (Farr & Kobrick, 2000; Shuttle Radar Topography Mission (SRTM) Spatial Metadata Dataset at [http://www.metrokc.gov/gis/sdc/radster/elevation/ShuttleRadarTopographyMission\(SRTM\)SpatialMetadata.html](http://www.metrokc.gov/gis/sdc/radster/elevation/ShuttleRadarTopographyMission(SRTM)SpatialMetadata.html)). The SRTM DEM has a horizontal datum of the World Geodetic System 1984 (WGS 84) and a vertical datum of NAVD 88. Before differencing, the NED DEM was over-sampled to match the horizontal datum and pixel size (30 m) of the SRTM data.

Nine global positioning system (GPS) benchmarks of known elevation (Mann & Freymueller, 2003) were used to assess the accuracy of the two DEMs (Table 2). The heights of these ground-truth points range from about 50 to about 1300 m (Table 2). Not surprisingly, we find that the SRTM heights better match the true elevations as represented by the GPS data than those of the NED. The height differences between GPS and NED or SRTM are independent of elevation. Since the height difference between GPS and NED (7.2 ± 7.4) is less than the stated accuracy of the NED DEM (15 m) (Gesch, 1994), we are able to confirm that, at least for these nine GPS points, the USGS NED DEM is within its stated accuracy of 15 m. However, as the NED DEM was produced from both contour and photogrammetric data, it is likely that accuracy over the top and the upper flank of Westdahl Volcano is less than the stated accuracy because these areas are covered by permanent snow or glaciers.

Both automated and manual techniques were used to map the three Westdahl lava flows of interest (1991–1992, 1964, and pre-1964). The processing was done using the ERDAS Imagine software. First, the region-growing technique (Haralick & Shapiro, 1985) was applied to discriminate the extent of the flows on the Landsat imagery. The region-growing algorithm is an image segmentation technique. It starts with a seed pixel, examines adjacent pixels, determines the most similar one, and includes it in the region if it

Table 1
SAR images used for this study

Date 1	Orbit 1
92/01/19	E1/02670
92/01/22	E1/02713
92/01/25	E1/02756
92/01/31	E1/02842
92/02/06	E1/02928
92/02/09	E1/02971

Dates are image acquisition times in yy/mm/dd format. Orbit numbers include the satellite ID (E1 = ERS1) and orbit on which the images were acquired.

Table 2
Comparison of elevation values for the nine GPS locations

X-coordinate (m)	Y-coordinate (m)	GPS (m)	NED (m)	SRTM (m)	SRTM–NED (m)	GPS–NED (m)	GPS–SRTM (m)
516586.3	6027823.5	55	43	55	12	12	0
529406.9	6051819.5	122	101	117	16	21	5
536145.9	6052535.0	153	153	154	1	0	–1
542551.3	6056051.5	187	185	189	4	2	–2
516419.5	6049880.5	449	436	449	13	13	0
529664.4	6043450.5	504	494	494	0	10	10
514270.8	6042816.0	621	613	615	2	8	6
517862.5	6036878.5	908	910	909	–1	–2	–1
520481.7	6045647.0	1304	1303	1306	3	1	–2
				Average	5.6	7.2	1.6
				STD	6.4	7.4	4.3

meets the predefined criteria. The process is repeated until the entire flow is adequately described. The degree of pixel similarity is defined by the Spectral Euclidean Distance value (Haralick & Shapiro, 1985). Second, a Lee filter (Lee, 1980) was applied to the radar images to reduce the amount of speckle and effectively preserve edges and features. A pseudo-lava flow map was then produced by thresholding the SAR amplitude imagery. Third, areas that were shown as lava flows by both the Landsat-7 and radar imagery were designated as lava flows. Based on vegetation and the lava

flow map produced previously (Dean et al., 2002), we then classified the lava flow areas as 1991–1992 flow, 1964 flow, or pre-1964 flow. Fourth, in areas where the Landsat-7 imagery and radar imagery do not agree, we delineated the lava flows by visual inspection. Fifth, in areas where the lava flows are covered by snow and ice, radar imagery provided the sole information for mapping the extent of the flows. The final map of areal distributions of the 1991–1992, 1964, and pre-1964 lava flows is shown in Figs. 1(d) and 2. Our estimates of the flow areas are 8.4, 9.2, and 7.3

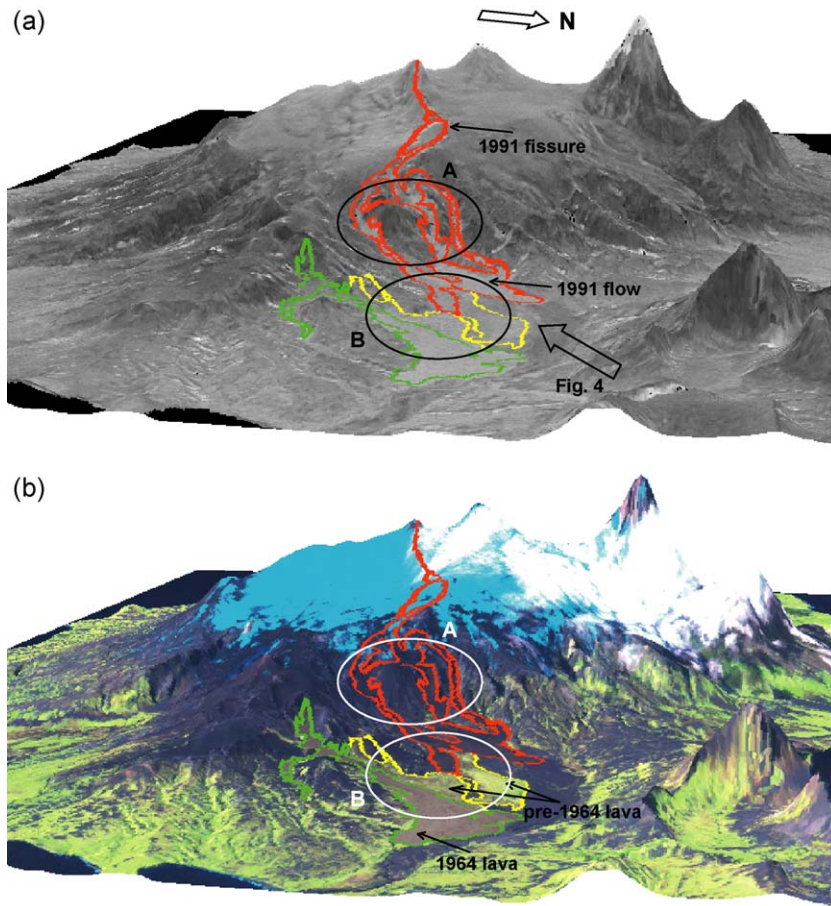


Fig. 2. Perspective view of the mapped lava flows superimposed on (a) the SAR image shown in Fig. 1(b) and (b) the Landsat-7 image shown in Fig. 1(c). The arrow in panel (a) shows the direction from which the photo in Fig. 4 was taken. The areas outlined by ovals A and B are discussed in the text.

km² for the 1991–1992, 1964, and pre-1964 flows, respectively (Table 3), assuming that the pre-1964 lava could have resulted from multiple eruptions and could also have been partially covered by the 1964 flow. Unfortunately, we do not have any image data acquired before 1964 to make any further investigation.

After all three lava flows had been defined, a three-dimensional (3D) view of the area was developed to verify the results. The 3D view was created using ArcScene, a module of the ArcGis software (ESRI, 2003). The ArcScene module contains a “steepest path” function, which allowed us to visualize how well the lava flows from the 1991–1992 eruption follow the topography of Unimak Island as defined by the NED DEM. The steepest path tool calculates the direction an object would take if released at a given point on the surface. The object will take the steepest path downhill until it reaches the perimeter of the surface model or it reaches a local topographic minimum. Despite the fact that the DEM was produced in 1970–1980s and is accurate to just 60 m horizontally and 15 m vertically, the “steepest path” confirms that the mapped lava flows conform remarkably well to the NED topography (Fig. 2).

To estimate the thickness of the 1991–1992 lava flow, we utilized the height difference between the NED and SRTM DEMs. The base data for the USGS NED DEM was acquired sometime during the 1970–1980s. The crater formed during the 1978 eruption is clearly visible in the NED DEM (Fig. 1d), so the DEM postdates that eruption. The following procedures were used to estimate the thickness of 1991–1992 flow.

(1) The horizontal misalignment between the two DEMs was checked using image cross-correlation to ensure that they were co-registered. The overall registration accuracy of the two DEMs is within 0.5 pixel.

(2) The height difference between the DEMs in several regions was computed and plotted to reveal any bias. Fig. 3(a)–(c) shows the histograms of height differences for these areas. In flat areas (Fig. 3a, b), the height difference has a mean of about 0 m and a standard deviation of less than 5 m. Over the southwestern flank of the volcano (Fig. 1c) where elevation values range from 0 to about 860 m, we find that the height difference is about -2 ± 5 m (Fig. 3c). We conclude that the DEM difference image has an overall relative vertical accuracy of about 5 m, which further confirms that the two DEMs are co-registered to each other to sub-pixel accuracy.

(3) We then analyzed the DEM difference in the glaciated summit area of Westdahl Volcano (Fig. 3d). The mean of the

DEM difference is about -11 m, suggesting the top of the volcano was lower in February 2000 than when the data for the NED DEM were acquired. Even though the mean difference of 11 m is similar to the accuracy of the DEMs, the negative value suggests that the difference is most likely due to the fact that the SRTM DEM was produced by C-band (5.6 cm wavelength) radar, which can penetrate glacial snow to about 12–35 m depth (Hoen & Zebker, 2000). This problem makes it difficult to estimate lava-flow thickness at the top of the volcano and in high-relief areas, and explains why some of the height difference values in these areas are negative (Fig. 3f). Another issue that complicates the thickness estimation is missing data values in the SRTM DEM, which are due to severe geometric distortion in areas of high relief or low phase coherence in the images used to produce the DEM (Farr & Kobrick, 2000; Smith & Sandwell, 2003). We masked all areas of missing data in the SRTM DEM. We also noticed that large values of DEM height difference distributed around the perimeter of the “holes”, which are probably caused by the application of a boxcar filter in SRTM processing (Smith & Sandwell, 2003).

(4) The histograms for the lower and the upper parts of the 1991–1992 lava flow are shown in Fig. 3(e) and (f), respectively. For the lower part, the height differences range from -10 to 80 m, with an average of 13 m. More than 95% of the height differences fall into the range of 0–30 m. Less than 2% of pixels have height differences between 50 and 80 m and they are probably outliers due to localized errors in the DEMs (e.g., Smith & Sandwell, 2003). For the upper part of the 1991–1992 flow, the values of height difference range from -50 to 30 m, with a mean of -10 m. Given the -11 m bias between the DEMs over glaciated summit area (Fig. 3d) and the -10 m mean for the height difference on the upper part of the 1991–1992 lava flow (Fig. 3f), we concluded that the thickness of the 1991–1992 flow in that area is not resolvable by this technique. Therefore, we only estimate the upper and lower bounds for the volume of the 1991–1992 lava flow.

(5) To determine the lower bound, we replaced height differences that were less than 0 m or greater than 30 m with 0 m, both in the upper and lower parts of the flow. The resulting volume estimate is 0.10 km³. For the upper bound, we replaced negative height differences with 30 m (the maximum plausible thickness) and obtained a volume estimate of 0.19 km³. Therefore, the total volume of the 1991–1992 lava flow is about 0.10–0.19 km³.

Table 3

Comparison of estimated areas of mapped lava flows

	Pre-1964 flow (km ²)	1964 flow (km ²)	1991–1992 flow (km ²)
This study	7.3	9.2	8.4
Dean et al. (2002)	8.97	9.9	3.8
Rowland et al. (1994)		12.7	6.3

4. Discussion and conclusion

Using SAR images acquired shortly after the 1991–1992 eruption and a Landsat-7 image acquired on September 27, 2000, we successfully discriminated the 1991–1992, 1964, and a pre-1964 lava flow at Westdahl Volcano. For the summit area and upper flanks of the volcano, radar images

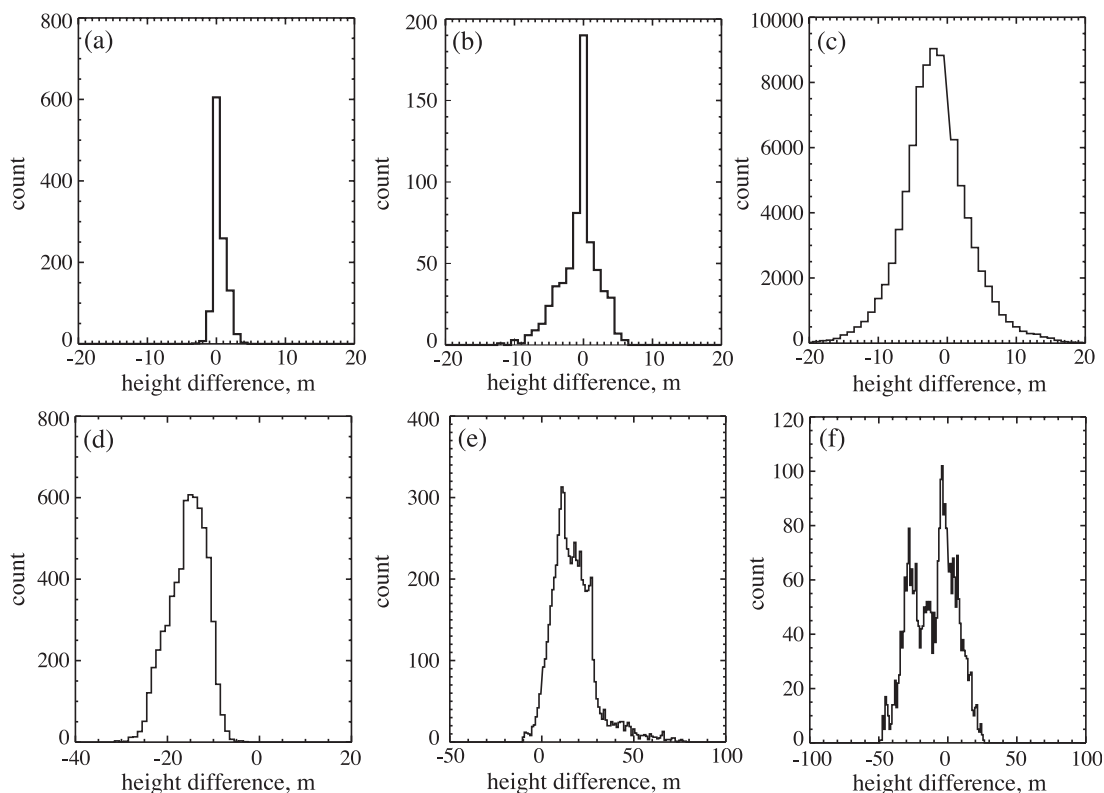


Fig. 3. Histograms of the DEM difference for selected areas: (a) a flat area on the pre-1964 lava flow, (b) a flat area on the 1964 lava flow, (c) an area on the southwestern flank of the volcano, (d) the glaciated summit area of the volcano, (e) the lower part of the 1991–1992 lava flow (elevation < 600 m), and (f) the upper part of the 1991–1992 lava flow (elevation > 600 m). The boxes in Fig. 1(b) outline the areas corresponding to the histograms in (a)–(d).

provided the sole source of information for mapping fissures, irregular channels, and lava flows that were quickly buried by snow and ice. On the lower flank and near the base of the volcano, the multispectral capabilities of Landsat-7 allow the flows to be distinguished based on vegetation cover. Two examples attest to the need for both data sets to accurately map the flows. The first is in the area outlined by oval A in Fig. 2, which includes both the 1991–1992 lava flow and lava or debris flows from earlier eruptions. Using only the Landsat-7 imagery, we could not easily distinguish the 1991–1992 flow from the others (Fig. 2b). However, this was possible by using the SAR image (Fig. 2) because the 1991–1992 flow is rougher than its surroundings and therefore produces stronger backscatter. The second example is from the area outlined by oval B (Fig. 2), which includes both the pre-1964 and 1964 flows. The SAR backscattering signals from the pre-1964 and 1991–1992 flows are very similar. However, the Landsat-7 image indicates that vegetation is denser on the pre-1964 lava flow than on the 1964 flow (Fig. 2b). We conclude that radar and optical images provide complimentary information associated with the different characteristics of the surface material and both are necessary to generate accurate lava flow maps.

Our estimate of the 1964 lava flow area is similar to that by Dean et al. (2002) (9.2 versus 9.9 km²), but our estimate

of the 1991–1992 flow is considerably larger (8.4 versus 3.8 km²) (Table 3). The reason for this difference is that the southern limb of the 1991–1992 flow was misclassified as being part of the pre-1964 flow in the analysis by Dean et al. Field observations confirm that this portion of the flow came from the 1991–1992 eruption (G. McGimsey, personal communication, 2003). An oblique aerial photograph taken at the end of the 1991–1992 eruption (Fig. 4) shows that the mapped extent of the 1991–1992 flow from this study (Figs. 1d and 2) agrees well with field observations.

Our estimate for the area of the 1991–1992 flow is a slightly larger than that by Rowland et al. (1994) (8.4 versus 6.3 km²), but our estimate for the 1964 flow is smaller (9.2 versus 12.7 km²). We postulate that in the analysis by Rowland et al. (1994) part of the pre-1964 lava flow was mistaken for the 1964 lava flow. The inclusion of multi-temporal SAR images and Landsat-7 data in our analysis permitted us to refine the estimates initiated by Rowland et al. (1994) and Dean et al. (2002). Our estimate of the average thickness of the 1991–1992 lava flow, 13 ± 5 m, agrees reasonably well with the reported thickness of 5–10 m from field observations (T. Neal, personal communication, 2002). Our estimate for the 1991–1992 flow volume is 0.10–0.19 km³. To derive the dense-rock equivalent volume, it is necessary to correct for void space in the flow due to vesiculation. The 1991–1992 lava flow is similar to



Fig. 4. An oblique aerial photograph showing the 1991–1992 lava flow at Westdahl Volcano. The photo was taken on February 13, 1992 by Fred Zeillemaker of the US Fish and Wildlife Service and provided by Game McGimsey of the Alaska Volcano Observatory. The direction from which the photo was taken is shown in Fig. 2a.

Hawaiian *aa* lava, which has vesicularity ranging from 10% to 75%. Our estimate for the dense-rock equivalent volume is therefore 0.06–0.17 km³.

The erupted volume estimates can be used not only to better document past eruptions, but also to anticipate future ones. For example, the volume of magma accumulation beneath Westdahl can be estimated from ground surface deformation as measured by interferometric SAR (InSAR) (Lu et al., 2000b, 2003b). It might be possible to constrain a time window for the next eruption by comparing the average lava volume produced by recent eruptions with the volume of magma accumulated in the reservoir since the most recent eruption (Lu et al., 2003b). Lu et al. (2003b) showed that the source of the 1991–1992 magma erupted at Westdahl was located about 6 km below the sea level and that the same source began to re-inflate soon after the eruption. The intervals between Westdahl's last three eruptions (1964, 1978, 1991–1992) have been about 13 years. The volcano has been inflating for more than 11 years since the 1991–1992 eruption and more than 0.04 km³ of magma has accumulated beneath the volcano as revealed by InSAR (Lu et al., 2003b). So, unless something has changed at Westdahl since 1991–1992, both the recent recurrence interval and the magma accumulation rate suggest that the next eruption might be expected before the end of this decade.

Finally, satellite-derived lava flow maps like those presented here for Westdahl can be used to generate, improve, or update existing geologic and lava-flow maps for frequently active volcanoes. A satellite-derived map can significantly reduce the time and effort required for fieldwork by showing the location and approximate boundaries of

new flows and by directing geologists to areas that require field checking or are of particular interest for some other reason.

Acknowledgements

ERS-1 SAR images are copyright ©1991 ESA, and provided by the Alaska Satellite Facility (ASF). This research was supported by funding from NASA (NRA-99-OES-10 RADARSAT-0025-0056), and in part by the USGS contract O3CRCN0001. We thank ASF for providing SAR data on a timely basis. We thank Game McGimsey and Tina Neal from the Alaska Volcano Observatory for sharing their insights regarding the Westdahl lava flows, and J. Groves for preparing the SRTM data. We are grateful for the detailed edits and comments by D. Dzurisin. We thank M. Poland, G. McGimsey, and two anonymous reviewers for providing constructive technical reviews of the manuscript.

References

- Abrams, M., Bianchi, R., & Pieri, D. (1996). Revised mapping of lava flows at Mount Etna, Sicily. *Photogrammetric Engineering and Remote Sensing*, 57, 1353–1359.
- Crisp, J. A. (1984). Rates of magma emplacement and volcanic output. *Journal of Volcanology and Geothermal Research*, 20, 177–201.
- Dean, K. G., Engle, K., Partington, K., Groves, J., & Dehn, J. (2002). Analysis of surface processes using SAR data: Westdahl Volcano, Alaska. *International Journal of Remote Sensing*, 23, 4529–4545.
- Dvorak, J., & Dzurisin, D. (1993). Variations in magma supply rate at Kilauea Volcano, Hawaii. *Journal of Geophysical Research*, 98, 255–268.

- ESRI, (2003). *ESRI ArcGIS*, 8.3. Redlands, CA: Environmental Systems Research Institute.
- Farr, T. G., & Kobrick, M. (2000). Shuttle Radar Topography Mission produces a wealth of data. *American Geophysical Union, EOS*, 81, 583–585.
- Gaddis, L. R., Mougini-Mark, P. J., & Hayashi, J. N. (1990). Lava flow surface textures: SIR-B radar image texture, field observations, and terrain measurements. *Photogrammetric Engineering and Remote Sensing*, 56, 211–224.
- Gesch, D. (1994). Topographic data requirement for EOS global change research. *USGS Open-File*, 62–94.
- Global Volcanism Network (1978). <http://www.volcano.si.edu/world/region11/aleutian/westdahl/var.html>, Smithsonian Institution Bulletin.
- Haralick, R. M., & Shapiro, L. G. (1985). Image segmentation techniques. *Computer Vision, Graphics, and Image Processing*, 29, 100–132.
- Hensley, S., Munjy, R., & Roen, P. (2001). Interferometric synthetic aperture radar (IFSAR). In: D. Maune (Ed.), *Digital elevation model technologies and applications: The DEM users manual* (pp. 143–206). Bethesda, MD: American Society for Photogrammetry and Remote Sensing.
- Hoen, E. W., & Zebker, H. A. (2000). Penetration depths inferred from interferometric volume decorrelation observed over the Greenland ice sheet. *IEEE Transactions on Geoscience and Remote Sensing*, 38, 2571–2583.
- Lee, J. S. (1980). Digital image enhancement and noise filtering by use of local statistics. *IEEE Transactions on Pattern Analysis and Machine Intelligence*, 2, 165–168.
- Legeley-Padovani, A., Mering, C., Guillaude, R., & Huaman, D. (1997). Mapping of lava flows through spot images—an example of the Sabancaya Volcano (Peru). *International Journal of Remote Sensing*, 18, 3111–3133.
- Lu, Z., Fielding, E., Patrick, M., & Trautwein, C. (2003a). Lava volume estimated by precision combination of multiple baseline spaceborne and airborne interferometric synthetic aperture radar: Application to the 1997 eruption of Okmok Volcano, Alaska. *IEEE Transactions on Geoscience and Remote Sensing*, 41(6), 1428–1436.
- Lu, Z., Mann, D., Freymueller, J., & Meyer, D. (2000a). Synthetic aperture radar interferometry of Okmok Volcano, Alaska: Radar observations. *Journal of Geophysical Research*, 105, 10791–10806.
- Lu, Z., Masterlark, T., Dzurisin, D., & Rykhus, R. (2003b). Magma-supply dynamics at Westdahl Volcano, Alaska, modeled from Satellite Radar Interferometry. *Journal of Geophysical Research*, 108 (B7), 2354 (10.1029/2002JB002311).
- Lu, Z., Wicks, C., Dzurisin, D., Thatcher, W., Freymueller, J., McNutt, S., & Mann, D. (2000b). A seismic inflation of Westdahl Volcano, Alaska, revealed by satellite radar interferometry. *Geophysical Research Letters*, 27, 1567–1570.
- Mann, D., & Freymueller, J. (2003). Volcanic and tectonic deformation on Unimak Island in the Aleutian Arc, Alaska. *Journal of Geophysical Research*, 108, 2108–2121.
- Miller, T. P., McGimsey, R. G., Richter, D. H., Riehle, J. R., Nye, C. J., Yount, M. E., & Dumoulin, J. A. (1998). Catalog of the historically active volcanoes of Alaska. *USGS Open-File Report*, 98-582, 104.
- NASA, (1999). Landsat-7 science data users handbook. (http://ftpwww.gsfc.nasa.gov/IAS/handbook/handbook_toc.html).
- Rowland, S. K., MacKay, M. E., Garbeil, H., & Mougini-Mark, P. J. (1999). Topographic analyses of Kilauea Volcano, Hawaii, from interferometric airborne radar. *Bulletin of Volcanology*, 61, 1–14.
- Rowland, S. K., Smith, G. A., & Mougini-Mark, P. J. (1994). Preliminary ERS-1 observations of Alaskan and Aleutian volcanoes. *Remote Sensing of Environment*, 48, 358–369.
- Sabins, F. F. (1997). *Remote sensing principles and interpretation*. (3rd ed.). New York, NY: Freeman.
- Smith, B., & Sandwell, D. (2003). Accuracy and resolution of shuttle radar topography mission data. *Geophysical Research Letters*, 30, 1467–1470.
- Toutin, T. (1996). Opposite side ERS-1 stereo mapping over rolling topography. *IEEE Transactions on Geoscience and Remote Sensing*, 34, 543–549.
- Ulaby, F. T., Moore, R. K., & Fung, A. K. (1986). *Microwave Remote Sensing: Active and Passive*, III. Boston, MA: Artech House.
- Wadge, G. (1977). The storage and release of magma on Mount Etna. *Journal of Volcanology and Geothermal Research*, 2, 361–384.
- Wood, C. A., & Kienle, J. (1990). *Volcanoes of North America: United States and Canada*, p. 354. Cambridge, MA: Cambridge University Press.
- Zebker, H., Rosen, P., Hensley, S., & Mougini-Mark, P. J. (1996). Analysis of active lava flows on Kilauea Volcano, Hawaii, using SIR-C radar correlation measurements. *Geology*, 24, 495–498.